Syst. Biol. 67(2):236–249, 2018

DOI:10.1093/sysbio/syx070
Advance Access publication August 26, 2017

Conflicting Evolutionary Histories of the Mitochondrial and Nuclear Genomes in New World *Myotis* Bats

ROY N. PLATT II[1], BRANT C. FAIRCLOTH[2], KEVIN A. M. SULLIVAN[1], TROY J. KIERAN[3], TRAVIS C. GLENN[3], MICHAEL W. VANDEWEGE[1], THOMAS E. LEE Jr.[4], ROBERT J. BAKER[1], RICHARD D. STEVENS[5], AND DAVID A. RAY[1,*]

[1]*Department of Biological Sciences, Texas Tech University, 2901 Main St, Lubbock, TX, USA;* [2]*Department of Biological Sciences and Museum of Natural Science, Louisiana State University, 202 Life Science Building, Baton Rouge, LA, USA;* [3]*Department of Environmental Health Science, University of Georgia, 206 Environmental Health Sciences Building, Athens, GA, USA;* [4]*Department of Biology, Abilene Christian University, 1600 Campus Ct. Abilene, TX, USA; and* [5]*Natural Resource Management, Texas Tech University, 2901 Main St, Lubbock, TX, USA*
[*]*Correspondence to be sent to: Department of Biological Sciences, Texas Tech University, Lubbock, TX, USA; E-mail: david.4.ray@gmail.com.*

Received 17 March 2017; reviews returned 31 June 2017; accepted 15 August 2017
Associate Editor: Matthew Hahn

Abstract.—The rapid diversification of *Myotis* bats into more than 100 species is one of the most extensive mammalian radiations available for study. Efforts to understand relationships within *Myotis* have primarily utilized mitochondrial markers and trees inferred from nuclear markers lacked resolution. Our current understanding of relationships within *Myotis* is therefore biased towards a set of phylogenetic markers that may not reflect the history of the nuclear genome. To resolve this, we sequenced the full mitochondrial genomes of 37 representative *Myotis*, primarily from the New World, in conjunction with targeted sequencing of 3648 ultraconserved elements (UCEs). We inferred the phylogeny and explored the effects of concatenation and summary phylogenetic methods, as well as combinations of markers based on informativeness or levels of missing data, on our results. Of the 294 phylogenies generated from the nuclear UCE data, all are significantly different from phylogenies inferred using mitochondrial genomes. Even within the nuclear data, quartet frequencies indicate that around half of all UCE loci conflict with the estimated species tree. Several factors can drive such conflict, including incomplete lineage sorting, introgressive hybridization, or even phylogenetic error. Despite the degree of discordance between nuclear UCE loci and the mitochondrial genome and among UCE loci themselves, the most common nuclear topology is recovered in one quarter of all analyses with strong nodal support. Based on these results, we re-examine the evolutionary history of *Myotis* to better understand the phenomena driving their unique nuclear, mitochondrial, and biogeographic histories. [Summary tree methods; concatenation; vespertilionidae; phylogenomics; UCE; ultraconserved elements.]

The bat genus *Myotis* (Order Chiroptera, Family Vespertilionidae) comprises more than 100 species that originated during the last 10–15 million years (Stadelmann et al. 2007), making it one of the most successful extant mammalian radiations. *Myotis* are distributed worldwide, excluding polar regions, and generally share a similar ecological niche: aerial insectivory. *Myotis* species often exhibit little morphological differentiation and, as a result, the rate of cryptic speciation within the genus is thought to be high. For example, specimens identified as *M. nigricans* and *M. albescens* form multiple paraphyletic lineages distributed throughout the phylogeny of Neotropical *Myotis* (Larsen et al. 2012). Confounding matters, the morphological variation that exists is often a poor indicator of species-level relationships. Early classifications of *Myotis* identified three major morphotypes (Findley 1972). Subsequent phylogenetic analyses of the mitochondrial cytochrome-b (*cytb*) gene demonstrated paraphyletic origins of each morphotype, suggesting frequent convergent evolution (Ruedi and Mayer 2001). These same analyses demonstrated that geography was a better predictor of phylogenetic relationship than morphology (Ruedi and Mayer 2001; Stadelmann et al. 2007).

The ability of mitochondrial markers to resolve a well-supported topology does not guarantee that the mitochondrial tree represents the species tree (e.g. see Willis et al. 2014; Li et al. 2016; Leavitt et al. 2017). The lack of recombination and uniparental inheritance of the mitochondrion means that it is transmitted as a single-genetic unit that is susceptible to evolutionary processes that may cause its history to diverge from the history of the species (Edwards and Bensch 2009). The most widely accepted phylogenies of *Myotis* rely heavily on mitochondrial data and even phylogenies containing nuclear data demonstrate an over reliance on mitochondrial markers for resolution, likely swamping out potentially conflicting signals from the nuclear genome. For example alignments of the nuclear *RAG2* and mitochondrial *cytb* contained 162 and 560 variable characters, respectively (Stadelmann et al. 2007). Despite these concerns, we find ourselves in a situation where our understanding of evolutionary relationships, our basis for conservation strategies, and our biogeographic hypotheses are all founded, almost entirely, on mitochondrial phylogenies.

Targeted sequencing of ultraconserved elements (UCEs; Faircloth et al. 2012) to collect sequence data from thousands of loci across the nuclear genome has resolved a number of difficult phylogenetic problems (e.g. see Faircloth et al. 2012; McCormack et al. 2013; Green et al. 2014; Faircloth et al. 2015; McGee et al. 2016). Here we used UCE baits to collect ~1.4 Mbp from >3600 nuclear loci in addition to random shotgun sequencing to collect full mitochondrial genomes in 37 taxa, primarily representing New World (NW) *Myotis*. Rather than analyzing each sequence data set once, or a handful of times, we chose to use a range of sampling, partitioning, and inference methods to fully explore phylogenetic tree

space of the nuclear and mitochondrial genomes. We recovered 294 trees representing 175 distinct topologies for the nuclear UCE data and 28 trees representing 14 distinct mitochondrial topologies. Our results show that, despite the range of trees recovered from each marker type, nuclear and mitochondrial markers occupy distinct regions in tree space. Given that the nuclear and mitochondrial trees are distinct from one another it is necessary to reevaluate hypotheses made based solely on the mitochondrial phylogeny.

Results

We used targeted sequencing of UCEs in 37 individuals (Table 1) to collect sequence data from 3648 nuclear loci which we assembled into concatenated alignments as large as 1.37 Mb. In addition, we assembled mitochondrial genomes for most taxa from random shotgun sequencing data. We then used the data to infer the phylogenetic history of New World *Myotis* using a range of locus sampling strategies, alignment partitioning methods, and phylogenetic inference methods.

Mitochondrial Assembly, Alignment, and Phylogenetic Inference

We generated an average of 5,498,440 paired reads per sample (min = 2,2370,68, max = 9,961,348) of random DNA sequence data for mitochondrial genome assembly. Assemblies varied in quality. Some were almost entirely complete while others were missing small regions. We were not able to assemble the entire mitochondrial control region for any of the samples. We found three premature stop codons in mtDNA protein coding genes. Subsequent manual alignment and validation suggested that these regions were miscalled by MitoBim, and we corrected the errors prior to analysis. Sequence coverage of the mitochondrial genomes averaged 58× (range >1×–297×).

The 37 mitochondrial protein coding, rRNA and tRNA genes were concatenated into an alignment of 15,520 bp containing 5007 informative characters. rRNA and tRNA genes were concatenated into an alignment containing 4157 bp containing 862 parsimony informative characters. Protein coding genes were concatenated into an alignment containing 11,363 bp or 3770 amino acids (aa) and containing 4145 or 509 parsimony informative characters, respectively. For the alignment containing all protein coding, rRNA and tRNA genes, 30 samples were ⩾ 90% complete, and alignments for five samples were 68–84% complete. Only 21% and 50% of nucleotide positions were present in the *M. albescens*[3] (TK 61766) and *M. levis* alignments, respectively.

When considering alignment type, partitioning strategy, and phylogenetic inference method we analyzed the mitochondrial data 28 ways as described in the Methods section. These analyses recovered 14 distinct topologies, the most common of which was recovered six times, all by analysis of the translated protein coding genes (Fig. 1a). Despite being the most common topology, bipartition frequencies and clade probability values were lower than nucleotide based data sets, as would be expected with more slowly evolving amino acid sequences. Analysis of RNA coding genes recovered two topologies depending on the method of phylogenetic inference. The remainder of the analyses recovered various trees without any pattern relating to partitioning scheme or inference method. A majority rule consensus tree for all 28 analyses is shown in Figure 1c. The mitochondrial consensus tree reflects previously reported mitochondrial phylogenies for *Myotis*. The New World *Myotis* are generally monophyletic splitting into Nearctic and Neotropical clades with the Old World taxon, *M. brandtii*, sister to the Neotropical clade. Ambiguity, represented by polytomies, is found only in terminal relationships.

UCE Assembly and Alignment, and Phylogenetic Inference

We averaged 3.29 million reads per sample after demultiplexing reads from the UCE-enriched, sequencing pool. These reads were assembled into an average of 5778 contigs per sample (min=1562 *M. nyctor*, max=11,784 *M. nigricans*[3]). Recovery rates for UCE loci varied across taxa. Of the 5500 loci in the Amniote probe set, we successfully recovered 3898 UCE loci, 3648 loci from five or more samples and 212 loci in all 37 samples (Table 2). On average, 3332 UCE loci were recovered per sample, ranging from 1106 (*M. nyctor*) to 4008 (*M. keaysi*). Repetitive sequences, identified via RepeatMasker searches, were minimal, occupying less than 0.02% of sites across all UCE alignments.

In all, 294 different combinations of alignment, partitioning, and inference method were used to identify 175 unique nuclear topologies. The most common tree was recovered 45 times (Fig. 1b). All nodes were highly-supported based on clade probability values and all but three nodes were highly supported with maximum likelihood bootstrap replicates. A consensus tree (Fig. 1d) of the 294 nuclear topologies resolves New World *Myotis* (and *M. brandtii*) as a single polytomy that excludes *M. volans* and represents a departure from previous mitochondrial phylogenies, including the one recovered herein. Comparison of the mitochondrial and nuclear consensus trees (Fig. 1c,d) reveals substantial differences in the relationships within the genus.

As noted above, we were concerned that phylogenetic error, sampling bias or other methodological factors may be driving the conflict between the mitochondrial and nuclear trees. To address this, we investigated the effects of matrix composition (or completeness) on phylogenetic inference by generating 10 alignments having varying levels of matrix completeness. Nine alignments were composed of loci with 15 to 95% (at 10% intervals) of taxa. The tenth alignment was composed of all loci which were recovered in 100% of specimens examined. For example, all loci that were represented

TABLE 1. Specimens examined

Species	Name herein	Museum identification or accession number	Number of UCE loci	Short read archive accession	Mitochondrial genome accession
Eptesicus fuscus	*fuscus*^{G}	GCA_000308155.1	2467	NA	KF111725.1
Eptesicus fuscus	*fuscus*	TK 178736	2849	SAMN06141755	MF143474
Myotis albescens	*albescens*^{1}	RDS 7889	2764	SAMN06141756	MF143471
Myotis albescens	*albescens*^{2}	QCAZ 9157	1185	SAMN06141757	MF143497
Myotis albescens	*albescens*^{3}	TK 61766	2872	SAMN06141758	MF143470
Myotis ater	*ater*	M4430	2774	SAMN06141760	MF143493
Myotis auriculus	*auriculus*	MSB 40883	2229	SAMN06141761	MF143486
Myotis brandtii	*brandtii*^{G}	GCA_000412655.1	2446	NA	KT210199.1
Myotis californicus	*californicus*	UMMZ 175828	2948	SAMN06141763	MF143469
Myotis davidii	*davidii*^{G}	GCA_000327345.1	2450	NA	KM233172.1
Myotis diminutus	*diminutus*	QCAZ 9168	3078	SAMN06141777	MF143481
Myotis dominicensis	*dominicensis*	TK 15624	2576	SAMN06141764	MF143467
Myotis evotis	*evotis*	MSB 47323	2586	SAMN06141765	MF143468
Myotis fortidens	*fortidens*	MSB 54941	2791	SAMN06141766	MF143483
Myotis horsfieldii	*horsfieldii*	MHNG 1926.039	3017	SAMN06141767	MF143494
Myotis keaysi	*keaysi*	TK 13525	3195	SAMN06141768	MF143477
Myotis keenii	*keenii*	UAM 113849	2723	SAMN06141769	MF143472
Myotis leibii	*leibii*	TK 24872	3119	SAMN06141770	MF143488
Myotis levis	*levis*	RDS 7781	2538	SAMN06141771	MF143482
Myotis lucifugus	*lucifugus*^{G}	GCA_000147115.1	2429	NA	KP273591.1
Myotis lucifugus	*lucifugus*	MSB 46679	2736	SAMN06141772	MF143491
Myotis melanorhinus	*melanorhinus*	TK 193888	3177	SAMN06141774	MF143489
Myotis nigricans	*nigricans*^{1}	QCAZ 9601	2854	SAMN06141775	MF143495
Myotis nigricans	*nigricans*^{2}	TK 194145	3159	SAMN06141776	MF143484
Myotis nyctor	*nyctor*	TK 151413	856	SAMN06141773	MF143498
Myotis occultus	*occultus*	MSB 121995	2957	SAMN06141778	MF143490
Myotis oxyotus	*oxyotus*	UMMZ RCO1013	3106	SAMN06141779	MF143479
Myotis riparius	*riparius*^{1}	TK 22688	2924	SAMN06141782	MF143473
Myotis riparius	*riparius*^{2}	TK 101723	2990	SAMN06141759	MF143475
Myotis riparius	*riparius*^{3}	TK 145199	2890	SAMN06141780	MF143480
Myotis ruber	*ruber*	MVZ 185692	2757	SAMN06141781	MF143478
Myotis septentrionalis	*septentrionalis*	TK 194420	2916	SAMN06141762	MF143487
Myotis thysanodes	*thysanodes*	07LEP	2821	SAMN06141783	MF143492
Myotis velifer	*velifer*	MSB 70877	2704	SAMN06141784	MF143499
Myotis vivesi	*vivesi*	MSB 42658	2469	SAMN06141785	MF143476
Myotis volans	*volans*	MSB 40886	2819	SAMN06141786	MF143496
Myotis yumanensis	*yumanensis*	TK 194144	2589	SAMN06141787	MF143485

Samples beginning with "GCA_" represent genome assemblies available through NCBI. Species with more than one sample are designated with a superscript. Specimens derived from whole genome alignments are designated with a superscript "G." MSB = Museum of Southwestern Biology; MVZ = Museum of Vertebrate Zoology; MHNG = Natural History Museum of Geneva; QCAZ = Pontificia Universidad Catolica del Ecuador Museo de Zoologia; TK = Texas Tech University Natural Science Research Laboratory; UAM = University of Alaska Museum of the North; UMMZ = University of Michigan Museum of Zoology.

in at least 15% of species ($n_{\text{taxa}} \geqslant 5$) were included in the alignment ($n_{\text{loci}} = 3648$). In the "100%" matrix, only loci which were identified in all species ($n_{\text{taxa}} = 37$) were included ($n_{\text{loci}} = 212$). Alignments were partitioned using three schemes: unpartitioned, individually partitioned by locus, or combined partitions. Alignment lengths, numbers of informative characters and number of partitions identified by PartitionFinder are available in Table 2. Resulting alignments were analyzed with Bayesian, maximum likelihood, and coalescent methods using RaxML, ExaBayes, ASTRID, ASTRAL-II, and SVDquartets as described in the Methods section. Bootstrap topologies stabilized in each alignment and partition combination within 150 replicates and all Bayesian runs converged in less than ten thousand generations. Unfortunately, computational limits forced us to abandon the individually partitioned, Bayesian analyses. In general, the same alignment produced the same topology regardless of inference method or partitioning scheme with the only exception being the terminal relationships of the *M. levis*/*M. albescens* clade in the combined versus unpartitioned Bayesian analysis of the 100% complete data matrix.

We also tested how locus length could affect phylogenetic discordance. To do so, trees were generated from data matrices incorporating UCE loci of differing lengths (Hosner et al. 2016). All 3648 loci were grouped into 10 separate bins based on locus length. The number of informative characters per bin ranged from 1115 to 6995 and the number of informative characters was

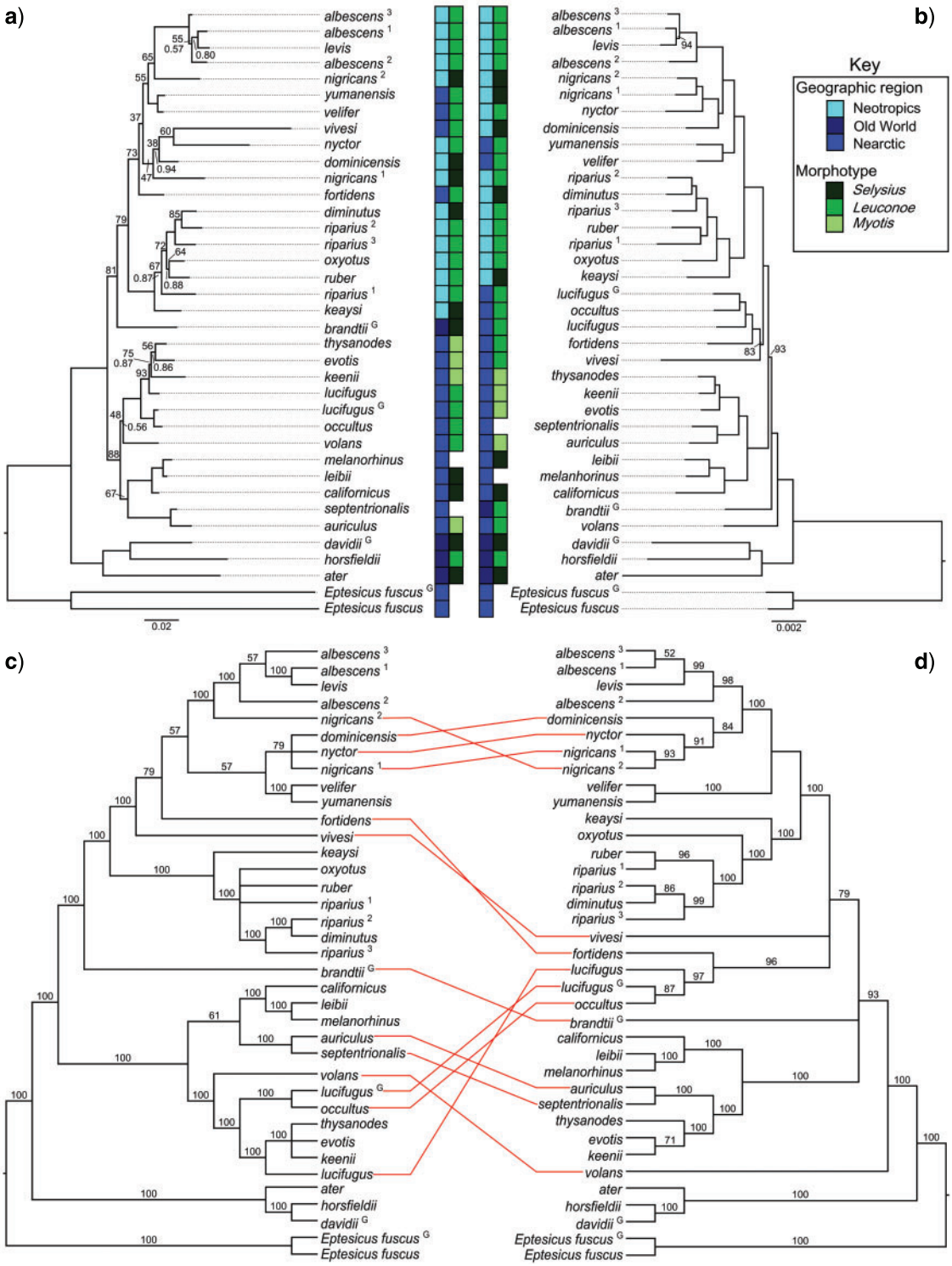

FIGURE 1. Comparison of nuclear and mitochondrial phylogenetic trees of *Myotis*. The most common mitochondrial (a) and nuclear (b) topologies. The mitochondrial topology arises from Bayesian and maximum likelihood analysis of the amino acid sequences portioned based on the PartitonFinder recommendations. The nuclear topology is from the 55% complete data matrix partitioned based on the recommendations of PartitionFinder. For clarity, bootstrap values greater than 95 and clade probability values greater than 0.95 have been omitted from the nuclear consensus tree. Majority-rule consensus trees from 28 mitochondrial (c) and 294 nuclear (d) topologies. Values above the branches in the consensus trees (c,d) are bipartition frequencies for that clade across all nuclear or mitochondrial topologies. Conflicting tips between data types (consensus nuclear vs. consensus mitochondrial) are indicated with red lines between the topologies. Biogeographic regions are color coded, as are subgeneric classifications based on morphotypes, as defined by Findley (1972). Species with more than one sample are designated with a superscript that is referenced in Table 1. Specimens derived from whole genome alignments are designated with a superscript "G."

TABLE 2. Matrix composition analysis

Matrix ID (% taxa with data from locus)	Min. num. of taxa	Number of loci characters	Parsimony-informative	Variable uninformative	Alignment length	Optimum partitions
15	5	3648	38,718	62,588	13,77,262	31
25	9	3379	37,894	57,672	12,60,248	37
35	12	3232	37,259	56,453	12,27,093	34
45	16	3064	36,539	54,782	11,87,492	31
55	20	2890	35,284	53,200	11,44,471	27
65	24	2668	34,373	51,148	10,91,620	27
75	27	2481	33,031	48,732	10,41,099	20
85	31	2034	29,179	41,711	903,903	16
95	35	1193	18,288	24,189	575,321	15
100	37	212	3480	4778	112,125	6

General alignment information. For a subset of analyses a series of alignments were generated based on the number of taxa represented by each locus. Thirty-seven taxa were examined so an alignment with all 37 taxa was considered 100% complete. Parsimony-informative characters make up a small portion of the total alignment. The optimum partitioning scheme was calculated with PartitionFinder.

correlated with average locus length (Supplementary Material Fig. 1 available on Dryad at http://dx.doi.org/10.5061/dryad.5g205). On average, only 2.6% of characters in each bin were parsimony-informative (Supplementary Material Fig. 1 available on Dryad at http://dx.doi.org/10.5061/dryad.5g205). Each of the ten length-based alignments recovered slightly different topologies. Terminal relationships were generally stable across analyses with the majority of differences between topologies found in the early bifurcations of *Myotis*. Generally, longer alignments produced well resolved and similar/identical topologies with significant nodal support regardless of the phylogenetic method or partitioning scheme used. In contrast, smaller data sets were more likely to yield unique topologies.

Given the goal of fully exploring nuclear tree space and generating as many reasonable nuclear UCE based topologies for comparison with the mitochondrial tree, we decided to randomly sample a limited number of nuclear UCE loci to create small alignments that would be more likely to result in unique topologies. We therefore randomly subsampled UCE loci to create 100 unique data sets of 365 loci. Loci were concatenated in each replicate data set and analyzed using maximum likelihood in RAxML. Of the 100 alignments analyzed, 80 unique topologies were generated (mean Robinson–Foulds distance = 4.3).

In addition to concatenation methods we explored phylogenetic tree space of the UCE data set using species tree methods. Normalized quartet scores from ASTRAL-II (Mirarab and Warnow 2015) analyses were consistent among all analyses, with scores ranging from 0.540 to 0.553, and the number of induced quartet gene trees ranging from 7,745,739 (100% complete 212 gene trees) and 63,042,410 (15% 3648 loci). SVDquartets (Chifman and Kubatko 2014) sampled all 66,045 quartets. On average, the total weight of incompatible quartets was 2.84%. Similar to the concatenated analysis, we inferred coalescent-based species from the same 100 subsamples of 365 loci described above. Despite being generated from the same underlying data, summary, and concatenation methods only recovered the same tree in 1 of 100 attempts.

Finally, we used weighted and unweighted statistical binning to combine individual gene trees into supergenes, estimate the supergene phylogeny, and then infer the species tree from the supergene trees. The 3648 loci were combined into 528 binned loci with 480 bins containing 7 loci each and 48 bins containing 6 loci each. Binning methods increases the normalized quartet scores from an average of 0.547 with gene trees to 0.672 for the binned-unweighted and 0.673 for the binned-weighted supergene trees. Given the relatively even distribution of loci into bins the negligible difference in quartet/species tree discordance between the unweighted and weighted supergene trees is expected. Binning methods have been shown to recover incorrect species trees under coalescent methods by altering gene tree frequencies. In addition, it is possible that support for incorrect trees can actually increase with the number of input gene trees (Liu and Edwards 2015). With these concerns in mind, both binning methods recovered the same topology which was the most common nuclear topology observed across all analyses (Fig. 1c).

Topological Comparisons

All mitochondrial and nuclear trees are available in Supplementary Material File 1 available on Dryad (http://dx.doi.org/10.5061/dryad.5g205). When visualizing all topologies in tree space, nuclear trees co-localized and were distinct from mitochondrial topologies (Fig. 2a). Comparisons of Robinson–Foulds symmetrical differences show 26 symmetrical differences between the most similar nuclear and mitochondrial trees (Fig. 2b). For comparison only 9 of 43,070 and 0 of 378 pairwise nuclear versus nuclear and mitochondrial versus mitochondrial tree comparisons, Figure 2c and d, respectively, exhibited more than 26 symmetrical differences.

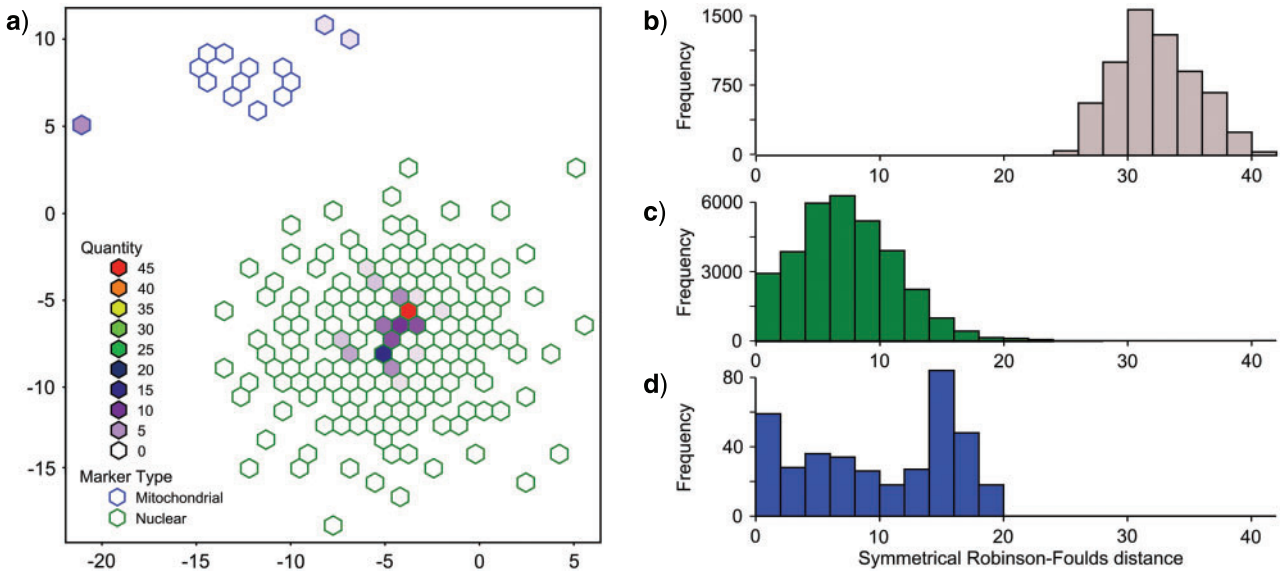

FIGURE 2. Comparison of mitochondrial and nuclear topologies (Fig. 1a). All trees recovered from mitochondrial and nuclear analyses were visualized in tree space using multidimensional scaling of Robinson–Foulds distances. Nuclear trees (green outlines) were clustered separately from mitochondrial trees (blue outlines). Robinson–Foulds distances between nuclear and mitochondrial trees (Fig. 1b), nuclear versus nuclear trees, (Fig. 1c) and mitochondrial versus mitochondrial trees (Fig. 1d) indicate the overall distinctions between the nuclear and mitochondrial topologies.

Of the 45 analyses that recovered the most frequently observed topology (Fig. 1b), 38 were Bayesian and RAxML searches that varied by matrix completeness and partitioning scheme. The fact that these analyses recovered the same topology is expected given that they are not independent. For example, a RAxML analysis of the 25% complete data set uses 1.26 Mb of the 1.38 Mb of data present in the 15% complete matrix, sharing 91% of the data. Analyses that directly varied the alignments and/or sampled less data (e.g. randomly sampling loci) were more likely to generate unique topologies than the nested analyses described above. Of the 200 analyses that randomly sampled UCE loci, 164 unique topologies were observed. This implies that when analyses of large data sets produce well-resolved trees with significant nodal support, sampling smaller portions of the data, may provide a mechanism for creating phylogenetic uncertainty not represented by typical tree scoring metrics.

DISCUSSION

We analyzed 3648 UCE loci and mitochondrial genomes of 37 *Myotis* bats and outgroups. The mitochondrial and nuclear UCE phylogenies recovered distinct topologies (Fig. 1), whether comparing the most commonly recovered or consensus topologies. Previous work with UCE loci demonstrated that support for deep divergences varied based on the number of loci examined (McCormack et al. 2013). Further, bootstrap replicates and clade probability values can be inaccurate metrics of nodal support (Douady et al. 2003, Hedtke et al. 2006). We varied the input data and phylogenetic parameters to produce a range of reasonable nuclear and mitochondrial topologies that may be more useful than overreliance on a tree resulting from one or two analyses. Rather than rejecting concordance between the two data types from a single analysis we took steps to analyze both data sets to generate many viable topologies to potentially reveal hidden overlap between marker types masked by phylogenetic error.

We recovered 175 and 14 unique nuclear and mitochondrial topologies from 294 and 28 analyses using multiple methodologies, sampling strategies, and phylogenetic parameters. By varying our phylogenetic methods we show that recovering a consistent topology is difficult even when using the same marker type, thus making it difficult to determine the "best" topology. Rather than choosing single trees to represent the nuclear and mitochondrial data, we use consensus trees to represent the ambiguity that is present through all analyses, in addition to phylogenies conforming to the most common topology (Fig. 1). Despite our efforts to identify as many plausible, distinct nuclear and mitochondrial trees as possible we were unable to recover overlapping topologies between marker types suggesting that nuclear UCE loci and the mitochondrial genomes of *Myotis* have distinct evolutionary histories.

A comparison of topologies in tree space illustrates the differenced in trees generated for each data set (Fig. 2a). Intramarker discordance, as measured by differences in nuclear versus nuclear or mitochondrial versus mitochondrial topologies is low. Pairwise comparisons of nuclear topologies contain an average of 8.3 symmetrical differences, mitochondrial comparisons contain an average of 10.8 differences. By contrast, pairwise differences between nuclear and mitochondrial topologies contain

an average of 33.3 symmetrical differences. The two most similar nuclear and mitochondrial topologies contain 26 symmetrical differences. Of the 43,072 pairwise comparisons of nuclear topologies, only 27 contain more than 26 symmetrical differences. Likewise of the 378 pairwise comparisons of mitochondrial topologies only one contains more than 26 symmetrical differences. These observations indicate that discordance between marker types (Fig. 2b) is much greater than within marker type (Fig. 2c,d). All but the most divergent nuclear topologies are more similar to each other than any nuclear versus mitochondrial comparison.

Conflict between mitochondrial and nuclear data may be driven by error in phylogenetic estimation or may reflect genuine discordance between the two marker types (Degnan and Rosenberg 2009; Huang et al. 2010). We relied on multiple tree-inference methods (e.g. summary vs. concatenation), manipulated phylogenetic parameters (e.g. partitioning strategy), and sampling criteria (e.g. loci sampled in all taxa) to minimize the impacts of phylogenetic error on the data sets. In most cases, varying parameters or methodologies generated unique topologies with minor differences. In most cases unique topologies resulted from rearrangements of a few terminal taxa. For example, placement of *M. volans* and *M. brandtii* was often either sister to the remaining New World *Myotis* or as an early bifurcation between the Nearctic and Neotropical clades. *Myotis vivesi* was at times found as sister to the clade containing *M. lucifugus*, *M. occultus*, and *M. fortidens* or as sister to the clade containing the neotropical *Myotis*.

Summary methods failed to recover the most common nuclear topology presented in Figure 1b except when loci were binned prior to gene tree estimation. Summary methods also tended to recover more unique topologies than concatenation methods when analyzing data from the same gene(s). For example, the random sample analyses recovered 80 unique topologies using concatenation (RAxML) and 89 unique topologies with summary methods (ASTRAL-II). This likely has to do with the limited number of informative characters per locus and by extension limited phylogenetic signal per gene tree (Supplementary Material Fig. 1 available on Dryad at http://dx.doi.org/10.5061/dryad.5g205). In these instances, limited phylogenetic signal per gene would likely lead to increased opportunity for phylogenetic error in gene tree estimation. Further supporting this idea, binning of compatible UCE loci may have indirectly increased phylogenetic signal resulting in the same topology that many of the concatenation analyses recovered. No other summary/coalescent method recovered this topology.

Previous studies that used primarily mitochondrial data recovered effectively the same relationships among *Myotis* as our mitochondrial analyses (Ruedi and Mayer 2001; Stadelmann et al. 2007; Roehrs et al. 2010; Larsen et al. 2012; Ruedi et al. 2013; Haynie et al. 2016). Differences between our tree and any single previously published trees are minor. For example, our tree agrees with Stadelmann et al. (2007) except in the placement of *M. septentrionalis* and *M. auriculus*. Our nuclear UCE topology places *M. septentrionalis* and *M. auriculus* sister to a clade containing *M. californicus*, *M. leibii*, and *M. melanorhinus*. Even though this placement of *M. septentrionalis* and *M. auriculus* disagrees with Stadelmann et al. (2007) it is the same relationship recovered by Haynie et al. (2016). Thus, even though there were some concerns and miscalled nucleotides in the MITObim assemblies, these inaccuracies have not caused the mitochondrial tree to deviate from the expectations derived from previous work. Given the consistency of our mitochondrial phylogeny with previously published and independently recovered topologies, we are confident that the mitochondrial phylogeny we recovered here, and by others, reflects the true mitochondrial tree. However, the mitochondrial topology may not adequately reflect the species history, particularly when considering the factors that cause incongruence between nuclear and mitochondrial gene trees. Causes of conflicting gene trees include horizontal transfer, gene duplication, introgressive hybridization, and incomplete lineage sorting. The rapid radiation of this clade as well as other biological factors suggests that some of these phenomena are more likely to have influenced the *Myotis* radiation than others.

Horizontal transfer of genes is thought to be rare in eukaryotes, but, vespertilionids in general (Thomas et al. 2011; Platt et al. 2014; Platt et al. 2016), and *Myotis* in particular (Pritham and Feschotte 2007; Ray et al. 2007; Ray et al. 2008; Pagan et al. 2010), have experienced horizontal transfer of DNA transposons. These events would not be reflected in our phylogeny because repetitive sequences were removed prior to phylogenetic analyses. More generally, gene duplications could create conflicting signal among individual UCE markers (e.g. comparing nonorthologous UCE loci), but the number of gene duplication events would have to be very high to impact enough of the 3648 UCE loci to confound the mitochondrial and nuclear phylogenies. Further ruling out gene duplication events as the dominant cause of conflicting phylogenetic signal is the fact that such events are likely depressed in *Myotis* as evidenced by their smaller genome size (~2.2 Gb) and trend towards DNA loss (Kapusta et al. 2017) combined with low rates of paralogy in UCEs in general (Derti et al. 2006).

Introgressive hybridization and reticulation could significantly influence the phylogenies of *Myotis* in a way that leads to conflicting signal between the nuclear and mitochondrial genomes (Sota 2002; Good et al. 2015). Hybridization in bats may be relatively common given their propensity to swarm at cave entrances for breeding purposes. In European *Myotis*, swarming has allowed for high degrees of hybridization between *M. brandtii, M. mystacinus, and M. alcathoe* (Bogdanowicz et al. 2012). Further, *M. evotis*, *M. thysanodes*, and *M. keeni* all experienced historical gene flow during their divergence (Carstens and Dewey 2010; Morales et al. 2016). We could also explain the differences between the mitochondrial

and nuclear UCE phylogenies if *Myotis* experienced extensive incomplete lineage sorting during their radiation. Two factors influence the rate of lineage sorting, the fixation rate and the speciation rate (Hudson et al. 2002). Increasing the time to fixation and/or decreasing the amount of time between cladogenic events will increase the likelihood of incomplete lineage sorting. *Myotis* are generally long-lived species (Dzeverin 2008) and underwent a rapid radiation between 5 and 10 MYA (Lack et al. 2010), suggesting that *Myotis* species are likely to experience higher levels of lineage sorting. The importance of these events—introgressive hybridization and incomplete lineage sorting—in driving the differences between the mitochondrial and nuclear phylogenies should be further explored.

Evolutionary History of Myotis

Our understanding of relationships within *Myotis* is heavily biased by mitochondrial data because nuclear markers were harder to collect and produced fewer informative sites (Ruedi and Mayer 2001; Stadelmann et al. 2007; Lack et al. 2010; Roehrs et al. 2010; Larsen et al. 2012; Ruedi et al. 2013; Haynie et al. 2016) or nuclear phylogenies with large numbers of makers contained limited numbers of taxa (Platt et al. 2015). Our UCE-based results indicate that nuclear trees vary substantially from the mitochondrial tree. Given that the nuclear and mitochondrial trees are different, we find it necessary to re-evaluate *Myotis* in the context of the nuclear data.

Paraphyly of *M. nigricans* and *M. albescens* was inferred from previous mitochondrial phylogenies. Larsen et al. (2012) identified a minimum of 4 and potentially 12 lineages in *M. albescens* and *M. nigricans*. Our sampling included three *M. albescens* and two *M. nigricans*, compared with Larsen's 17 and 29 samples. Despite different mitochondrial and nuclear topologies overall, our mitochondrial and nuclear phylogeny recovered the same paraphyletic clade of three *M. albescens* samples and *M. levis*. Close relationships between these taxa were found in previous work and are expected. More importantly we did not find that *M. albescens* was paraphyletic across much of neotropical *Myotis*. We also found that *M. nigricans* is monphlyletic in the nuclear tree, but paraphyletic in the mitochondrial tree. These results from *M. nigricans* and *M. albescens* are interesting but further inference is limited due to low sample sizes of these taxa.

The original subgeneric taxonomy of *Myotis* was based on three morphotypes that were later shown to be the result of convergent evolution (Ruedi and Mayer 2001). If lineage-sorting affected the mitochondrial phylogeny, it is possible that the morphotypes truly are monophyletic. However, superimposing the previous subgeneric/morphological classification onto the species tree shows an interspersed distribution of morphotypes throughout the most common and consensus nuclear topologies (Fig. 1a,b). Many strongly supported terminal relationships link species with different morphotypes. Based on these results, it appears that the three major morphotypes in *Myotis* are indeed a result of convergent evolution, as suggested by previous work (Ruedi and Mayer 2001; Stadelmann et al. 2007) despite the conflicting mitochondrial and nuclear phylogenies recovered.

Among the more dramatic differences between the nuclear and mitochondrial topologies is the placement of *M. volans* and *M. brandtii* as sister to all New World taxa by the nuclear data. Our mitochondrial analyses place *M. volans* within a Nearctic clade and *M. brandtii* directly inbetween the Nearctic and Neotropical bifurcations (Fig. 1a,c) as has been previously reported (Stadelmann et al. 2007). In contrast the consensus UCE tree (Fig. 1d) places *M. brandtii*, a species distributed throughout the Old World, within a polytomy at the base of the New World *Myotis* radiation and *M. volans* sister to all New World *Myotis* (including *M. brandtii*). The placement of *M. brandtii* in the nuclear UCE consensus tree does not necessarily contradict the mitochondrial phylogeny since it is an unresolved polytomy. However, it is worth noting that the most commonly recovered nuclear topology (Fig. 1b) places *M. brandtii* sister to all New World *Myotis* (excluding *M. volans*). This relationship would more closely affiliate *M. brandtii* with other Old World taxa. The placement of *M. volans* as sister to all New World taxa (including *M. brandtii*) in the most common nuclear tree is a significant departure from previous work and, at first glance, does not make as much sense in a biogeographic framework. *Myotis volans* is distributed across western and northwestern North America as far as far north as Alaska. *Myotis brandtii* is distributed across much of Northern Europe and into the extreme eastern regions of Siberia. The key may lie in understanding the biogeography and phylogenetics of a third species, *M. gracili*s, a species that we were unfortunately unable to include.

Myotis gracilis, along with *M. brandtii*, are the only two *Myotis* geographically distributed in the Old World, but phylogenetically affiliated with the New World *Myotis* (Stadelmann et al. 2007). If future work verifies the sister relationship between *M. brandtii* and *M. gracilis*, then we can envision a scenario where *M. gracilis, M. brandtii,* and *M. volans* are the result of cladegenic events that occurred during the transition of *Myotis* from the Old World to the New World. It is important to remember that this interpretation relies on a fairly dramatic departure from the currently accepted mitochondrial relationships of *M. volans* (represented here by a single sample) to other *Myotis* species and abandons the nuclear UCE consensus tree for the most frequently recovered UCE topology. In addition, our taxonomic sampling excludes *Myotis* species from the Old World, Ethiopian clade, the sister clade to New World *Myotis* (Ruedi and Mayer 2001; Stadelmann et al. 2007; Lack et al. 2010; Ruedi et al. 2013). Taxa from the Ethiopian clade are needed to properly root the New World *Myotis* clade and understand its biogeographic origins. With these caveats in mind, the hypothesis presented here should be viewed as highly

speculative. Increasing the number of sampled *Myotis* lineages will shed additional light on this hypothesis.

Other taxa with conflicting positions between marker types include the *M. lucifugus* + *M. occultus* clade, *M. fortidens*, and *M. vivesi*. In general, these relationships are characterized by very short branches (Fig. 1d) and are the most likely to be affected by incomplete lineage sorting or limited phylogenetic information. This could explain the strong support with the mitochondrial tree compared with the nuclear species tree, while allowing for a number of nuclear loci to disagree with the species tree, as well.

There are a number of monophyletic groups identified with nuclear data (Fig 1a) that share general morphologies. For example, all of the long-eared bats (*M. septentrionalis*, *M. auriculus*, *M. evotis*, *M. thysanodes*, and *M. keenii*) represent a monophyletic group of higher elevation, forest-dwelling species that glean insects off of surfaces (Fitch and Shump 1979; O'Farrell and Studier 1980; Warner 1982; Manning and Jones 1989; Caceres and Barclay. 2000). The group represented by *M. fortidens*, *M. lucifugus*, and *M. occultus* represent a relatively long-haired form of *Myotis*. While having a distinct dental formula, *fortidens* was historically described as a subspecies of *M. lucifugus* (Miller and Allen 1928), and *M. occultus* has alternately represented its own species or been considered a subspecies of *lucifugus* (Hollister 1909; Valdez et al. 1999; Piaggio et al. 2002). The clade consisting of *M. keaysi*, *M. oxyotus*, *M. ruber*, *M. riparius*, and *M. diminutus* represents a neotropical group of primarily woolly haired bats (LaVal 1973). None of these relationships are monophyletic in the consensus or most common mitochondrial topologies. If the mitochondrial genome has been subjected to phenomena that obscure the true species tree then these species groups, along with their synapomorphic morphological features, can be reevaluated.

Conclusions

Relationships within *Myotis*, which until now have relied heavily on mitochondrial data, served as the basis for species identification (Puechmaille et al. 2012), evolutionary hypotheses (Simões et al. 2007), and even conservation recommendations (Boyles and Storm 2007). Previous studies using nuclear data have largely been uninformative or utilized too few samples to draw definitive conclusions. Trees estimated from ~3650 nuclear loci and 295 phylogenetic analyses recovered 175 topologies, none of which are congruent with the mitochondrial phylogeny of *Myotis*. Conflict between the mitochondrial and nuclear trees as well as among individual nuclear loci suggest that the *Myotis* radiation may have been accompanied by high levels of incomplete lineage sorting and possible hybridization. Rather than placing emphasis on the mitochondrial tree, it may be more appropriate to consider it for what it really is: a single gene on par with a single-UCE locus, albeit one with many more phylogenetically informative characters. If true, then the mitochondrial genome is as likely to reflect the true species tree as any single-UCE locus chosen at random. Phenomena such as lineage sorting, reticulation, and introgression have likely influenced the genomes of *Myotis* and should be accounted for in subsequent work. It is possible that the *Myotis* radiation is more accurately reflected as a hard polytomy or a phylogenetic network rather than a strictly bifurcating phylogeny.

Materials and Methods

Taxon Selection

Taxa were selected to span the major phylogenetic break points with emphasis on the Nearctic and Neotropical bifurcation as recovered in previous mitochondrial phylogenies (Stadelmann et al. 2007; Ruedi et al. 2013). In addition, multiple individuals morphologically identified as *M. nigricans* and *M. albescens* were included to test for paraphyly as suggested by Larsen et al. (2012). Three Old World species of *Myotis* and the outgroup, *Eptesicus fuscus*, were included to root phylogenetic analyses. All field identifications were confirmed from museum-voucher specimens. Information for all specimens examined is available in Table 1.

Library preparation, sequencing, and processing

Genomic DNA was extracted from 33 samples using either a Qiagen DNEasy extraction kit or a phenol-chloroform/ethanol precipitation. DNA was fragmented using the Bioruptor UCD-300 sonication device (Diagenode, Denville, NJ, USA). Libraries were prepared using the Kapa Library Preparation Kit KR0453-v2.13 (Kapa Biosystems, Wilmington, MA, USA) following the manufacturer's instructions with five minor modifications. First, we used half volume reactions. Second, subsequent to end repair, we added Sera-Mag Speedbeads (Thermo-Scientific, Waltham, MA, USA; prepared according to Glenn et al. 2016) at a ratio of 2.86:1 for end repair cleanup. Third, we ligated universal iTru y-yoke adapters (Glenn et al. 2016) onto the genomic DNA. Fourth, following adapter ligation, we performed one postligation cleanup followed by Dual-SPRI size selection using 55 µL of speedbead buffer (22.5mM PEG, 1M NaCl) and 25 µL of Speedbeads. Finally, we performed a PCR at 95°C for 45 s, then 14 cycles of 9 °C for 30 s, 60°C for 30 sec, 72°C for 30 s, then 72°C for a 5 min final extension and a 12°C hold using iTru5 and iTru7 primers to produce Illumina TruSeqHT compatible libraries (Glenn et al. 2016).

Libraries were quantified on a Qubit 2.0 (Life Technologies) and 83 ng from each library was added to create 5 pools of 6 or 7 libraries each. We then split the pools in two. One subsample was enriched for UCE loci, the other was not. UCE loci in the enriched library pools were captured using Tetrapods 5K version 1 baits from MYcroarray (Ann Arbor, MI, USA) following their MYbaits protocol v. 2.3.1 with overnight incubations (Faircloth et al. 2012). Enriched libraries were quantified with a

Qubit and pooled with other unrelated samples prior to sequencing on an Illumina HiSeq 3000 to produce paired-end reads of $\leqslant$ 151 bases. The unenriched samples were sequenced on a separate run using a single lane of Illumina HiSeq 2500. All samples were demultiplexed with Illumina's fastq2bcl software. Reads were quality filtered by removing any potential adapter sequence and trimming read ends once the average Phred quality over a four-base window score dropped below 20 using the Fastx toolkit (Gordon and Hannon 2010).

Assembly, Annotation, and Phylogenetic Analysis of the Mitochondrial Genome

Raw reads from the unenriched libraries were used to generate mitochondrial genomes via MitoBim (Hahn et al. 2013). This program used MIRA (Chevreux et al. 1999) to map reads to a *M. brandtii* reference mitochondrial genome (Genbank accession number KT210199.1). Alternative methods of mitochondrial genome assembly were used when MitoBim assembly failed. These taxa include *M. albescens* (TK61766), *M. albescens* (TK 101723), *M. albescens* (RDS 7889), *M. fortidens*, M. *keeni*, *M. melanorhinus*, *M. nigricans* (QCAZ 9601), *M. septentrionalis*, *M. simus*, *M. velifer*, and *M. volans*. For these samples, we first identified reads that were mitochondrial in origin using BLAST searches against the *M. brandtii* mitochondrial genome (KT210199.1). Those reads were assembled using Trinity v2.2.0 with the "–single" option to treat reads as unpaired. For taxa where we used NCBI genome assemblies to recover UCE loci *in silico* mitochondrial genomes from genbank were used to in the mitochondrial analyses GenBank as follows: *M. brandtii* (KT210199.1), *E. fuscus* (KF111725.1), *M. lucifugus* (KP273591.1), and *M. davidii* (KM233172.1).

Once assembled, each mitogenome was annotated via MITOS (Bernt et al. 2013). Annotated genes were manually validated via BLAST to confirm sequence identity and length. Protein coding genes were checked for stop codons using EMBOSS's transeq program (Rice et al. 2000). When a stop codon was found, we used the raw reads to verify the sequence. We used BWA v0.7.12 (Li and Durbin 2009) to align the reads to the Mitobim assembled mitogenome to verify base calls from Mitobim. The protein coding rRNA and tRNA genes from each assembly were aligned using MUSCLE and concatenated into three different alignments containing only protein coding genes, only rRNA and tRNA genes, or all protein coding and RNA genes. A fourth alignment of all protein coding genes was translated to amino acids and concatenated into a single alignment.

Several different partitioning schemes were examined for each of the mitochondrial alignments. Alignments were either partitioned by gene, by codon, or by gene type (rRNA and tRNA vs. protein coding). Genes were partitioned individually except in the instances where two genes overlapped. These regions were partitioned separately from the individual genes resulting in three partitions for the two genes: a partition for gene A, a partition for gene B, and a partition for the overlapping nucleotides of gene A and B.

Assembly and Phylogenetic Analysis of Nuclear UCEs

Quality filtered raw sequence reads from the UCE-enriched libraries were assembled into contigs using the Trinity assembler (Grabherr et al. 2011) with a minimum kmer coverage of 2. We used Phyluce to identify those assembled contigs that were UCE loci. We also harvested UCE loci from *E. fuscus* (GCA_000308155.1), *Myotis brandtii* (GCA_000412655.1), *M. davidii* (GCA_000327345.1), and *M. lucifugus* (GCF_000147115.1) genome assemblies using the Phyluce package (Faircloth 2016). Once extracted from Trinity and genome assemblies, we aligned all UCE loci using MAFFT (Katoh et al. 2002) and trimmed the aligned data with gBlocks (Castresana 2000). Repetitive sequences (i.e. transposable elements) in each alignment were identified with RepeatMasker and trimmed where found.

Each alignment was analyzed using three different partitioning schemes. Unpartitioned alignments were simply concatenated UCE loci treated as a single unit. These alignments are referred to herein as "unpartitioned." Fully partitioned alignments were concatenated alignments mitochondrial genes that were partitioned by locus. These alignments are referred to herein as "locus partitioned." Finally, PartitionFinder v1.1.1 (Lanfear et al. 2012) was used to combine individual loci into an optimal partitioning scheme. The combined partitioning schemes for each alignment were identified with PartitionFinder v1.1.1 (Lanfear et al. 2012). Rather than searching for best-fit substitution models for each locus or partition, the GTR+Γ model of sequence evolution was assigned to all loci (Darriba and Posada 2015) except in the case of amino acid alignments where the MtMam model was used. Initial trees for PartitionFinder were generated using RAxML v7.4.1 (Stamatakis 2006) with linked branch lengths. Partitioning schemes were heuristically searched using the hcluster algorithm. Partitioning schemes were chosen using the Bayeisan information criterion.

Finally, each alignment and partitioning scheme was analyzed using Bayesian inference and maximum likelihood phylogenetic methods. Bayesian phylogenies were generated with the MPI version of ExaBayes (v1.4.1) using 4 independent runs of 4 chains each. ExaBayes runs were terminated after 10 million generations only if the average standard deviation of split frequencies was less than 0.01. The first 25% of samples were discarded after which every 1000th generation was sampled. Proper sampling, post burn-in was inspected via Tracer v1.6. (Rambaut and Drummond 2014) and effective sample sizes greater than 200 were considered acceptable. Posterior probability values greater than 95% were considered to be significant. RaxML (v8.1.3) was used to estimate and score the maximum likelihood phylogeny with the rapid bootstrapping option and 10,000 bootstrap replicates. We define strongly supported bipartitions as those present

in 95–100% of bootstrap replicates and moderately supported bipartitions are present in 85–95% of bipartitions (Wiens et al. 2008).

Alignment types.—Different combinations of UCE loci were used to create unique matrices based on 1) locus distribution, 2) locus length, or 3) random locus sampling. The first set of alignments (locus distribution) was determined by the number of taxa represented in the UCE alignments (phyluce_align_get_only_loci_with_min_taxa; Faircloth 2016), or degree of completeness. Matrices were constructed using loci which were present in 100% (number of specimens, $n=37$), 95% ($n=35$), 85% ($n=31$), 75% ($n=27$), 65% ($n=24$), 55% ($n=20$), 45% ($n=16$), 35% ($n=12$), 25% ($n=9$), and 15% ($n=5$) of specimens examined. These 10 groups were nonexclusive, so a locus that was assembled in all specimens (100% complete) would also be included with loci present in only 55% of specimens. On the other hand, a locus found in only 55% of specimens would not be included in the 100% complete data set. Each set of UCE alignments was concatenated using phyluce_align_format_nexus_files_for_raxml and a nexus character block was created using the phyluce_align_format_nexus_files_for_raxml—charsets option. These data sets then served as the basis for downstream phylogenetic analyses. For example, when a partitioning methodology (discussed below) was tested, it was performed for each of the 100%, 95%, 85%, etc. alignments. In addition to partitioning schemes, the effect of missing data was examined using Bayesian and maximum likelihood methods.

The second alignment criterion combined UCE loci of similar sizes. Pervious coalescent analyses of UCE data showed that subsampling the most informative loci can result in different topologies (Meiklejohn et al. 2016). Rather than using coalescent based analyses, we used concatenation of UCE loci to identify different topologies based on length. Under these assumptions, UCE loci were sorted into 10 groups based on their length and the predicted correlation between length and number of informative characters was confirmed (Supplementary Material Fig. 1 available on Dryad at http://dx.doi.org/10.5061/dryad.5g205). UCE loci in the same size cohort were combined into a single alignment, partitioned by locus, and analyzed with RAxML using the methods described below.

The final set of alignments was generated by random sampling of UCE loci. In large phylogenetic analyses, systematic error can result in highly supported, but incorrect topologies due to compounding of nonphylogenetic signal (Rodríguez-Ezpeleta et al. 2007). By randomly reducing the data set and replicating the maximum likelihood analyses, we can reduce the potential effects of compounding error. Roughly 10% of the data set, 365 loci, were randomly sampled, concatenated, and partitioned by locus to create 100 new alignments, which were then analyzed with RAxML using the methods described below.

Partitioning strategies.—Alignments were analyzed using three different partitioning schemes—single, locus, and combined—similar to the mitochondrial partitioning schemes described above. Unpartitioned alignments were simply concatenated UCE loci treated as a single-genetic unit. Rather than searching for best-fit substitution models for each UCE locus or partition, the GTR+Γ model of sequence evolution was assigned to all loci (Darriba et al. 2015). Initial trees for PartitionFinder were generated using RAxML v7.4.1 (Stamatakis 2006) with linked branch lengths. Partitioning schemes were heuristically searched using the hcluster algorithm and the best scheme was chosen using the Bayesian information criterion.

Inference methods.—Phylogenetic trees were generated with three different phylogenetic inference methods across five different inference implementations including concatenation and summary tree methods.

Maximum likelihood trees were inferred for each alignment and partitioning combination using RAxML v8.1.3 (Aberer et al. 2014). The best scoring (lowest -lnL) tree from each data set was identified from 100 random starting trees and bootstrapped 100 times using the GTR+Γ in both cases. The autoMRE function in RAxML v8.1.3 was used to determine the need for additional bootstrap replicates beyond the initial 100 (Pattengale et al. 2009). A stopping criterion was set *a priori* if the weighted Robinson–Foulds distance was less than 5% in 95% of random permutations of computed bootstrap replicates (Pattengale et al. 2009). If necessary, an additional 100 bootstrap replicates were computed until the convergence stopping criteria were met. Finally, bipartition frequencies of bootstrap replicates were drawn onto the best scoring tree from the initial RAxML searches for each of the respective data sets. Alignments based on UCE length or randomly sampled were analyzed using slightly different methods. In both cases UCE loci were partitioned individually and nodal support was calculated using 100 bootstrap replicates using the RAxML fast-bootstrapping option. For all maximum likelihood analyses, we define strongly supported bipartitions as those present in 95–100% of bootstrap replicates and moderately supported bipartitions are present in 85–95% of bipartitions (Wiens et al. 2008).

Bayesian analyses were conducted using ExaBayes v1.4.1 (Aberer et al. 2014). For all Bayesian analyses four independent runs of four chains each were run in parallel for a minimum of one million generations sampling every thousandth generation and applying a GTR+Γ substitution model for each partition. After one million generations, analyses continued until the standard deviation of the split frequency between chains was less than 0.01. The "-M 3" option was used to reduce the memory footprint of all ExaBayes runs. Proper sampling, post burn-in, was inspected via Tracer v1.6. (Rambaut et al. 2014). Effective sample sizes greater than 200 were considered acceptable. Posterior probability values greater than 95% were considered significant. An extended majority rule consensus tree was created

from all trees after the first 25% of trees were discarded using TreeAnnotator v1.7.0 (Rambaut et al. 2013) and parameter estimates across all runs were calculated with Tracer v1.6 (Rambaut et al. 2014).

Species trees were calculated from gene trees for individual UCE loci recovered in five or more taxa using the GTR+Γ substitution model and fast bootstrapping (-f a) option in RAxML and 1000 bootstrap replicates. In general, gene trees were classified based on the degree of completeness (i.e. number of taxa represented) similar to the way we treated individuals as described above.

Species trees were estimated and bootstrapped using three different programs. ASTRAL-II v4.10 (Mirarab et al. 2015) was used to build a summary tree. Support values for bipartitions in the tree were generated from 100 bootstrap replicates using site as well as site and locus resampling (Seo 2008). Species trees were estimated from ASTRID v1.4 (Vachaspati et al. 2015) using bionj and bootstrapped for 100 replicates. SVDquartets (Chifman et al. 2014), as implemented in PAUP v4.0a150 (Swofford 2003), was used to estimate a species trees from a random subset of 200,000 quartets and 1000 bootstrap replicates.

UCE loci are relatively short markers with few informative characters from which to build gene trees. Errors in gene tree estimation may reduce the accuracy of summary methods and phylogenetic inference (Liu et al. 2009, Leaché Rannala 2011, DeGiorgio and Degnan 2014, Mirarab et al. 2016). We used weighted and unweighted statistical binning to combine genes into compatible supergenes, increasing the number of informative characters per "locus" and reducing the phylogenetic error (Mirarab et al. 2014, Bayzid et al. 2015). The gene trees used for the summary tree methods described above were used rather than re-estimating trees. Bifurcations supported by more than 50% of the bootstrap replicates were retained for each gene tree. Alignments from compatible trees were concatenated into a single-supergene alignment. Trees for supergenes were estimated using RAxML. The best trees for each supergene, as defined by log likelihood score, were retained from 500 searches. Bipartition support was estimated from 500 bootstrap replicates. For all analyses, the GTR+Γ model of substitution was used and each gene in the supergene alignment was partitioned separately. The resulting supertrees were then used for species tree estimation using ASTRAL-II. For the unweighted analysis, all supertrees were included in the pool of trees. For the weighted analysis, supertrees were weighted according to the number of genes combined in the supergene alignment. For example, if a supergene was a composite of six genes, the supertree was present six times compared with a composite of five genes which would be represented only five times. Support for the weighted and unweighted species trees was estimated by site and locus resampling (Seo 2008) for 100 bootstrap replicates in ASTRAL-II.

Topological comparisons.—Trees recovered from all analyses were compared with each other in order to quantify the differences between topologies. Branch lengths have different meanings based on the type of analysis. For example, ASTRAL-II branch lengths are representative of coalescent units and ASTRID does not calculate branch lengths. For accurate tree comparisons, branch lengths were stripped from all trees. Pairwise unweighted Robinson–Foulds distances were calculated among all trees. Robinson–Foulds distances were transformed into two dimensions using the stochastic CCA algorithm for nonlinear dimension reduction in TreeScaper v1.09 (Huang et al. 2016). Coordinates were then visualized in R using hexagonal binning in the hexbin library v1.27.1 (Lewin-Koh 2011). Nuclear and mitochondrial 50% majority rule consensus trees were generated with PAUP v4.0a150 (Swofford 2003).

Supplementary Material

Data available from the Dryad Digital Repository: http://dx.doi.org/10.5061/dryad.5g205.

Funding

This work was supported by the National Science Foundation [DEB-1355176]. Additional support was provided by College of Arts and Sciences at Texas Tech University.

Acknowledgments

We would like to thank the following museums, collection managers, and collaborators for the tissue loans necessary to complete this work: Joseph Cook (Museum of Southwestern Biology), Museum of Vertebrate Zoology, Manuel Ruedi (Natural History Museum of Geneva), Santiago Burneo (Pontificia Universidad Catolica del Ecuador Museo de Zoologia), Heath Garner, Robert Bradley and Caleb Phillips (Texas Tech University Natural Science Research Laboratory), Link Olson (University of Alaska Museum of the North), and Cody Thompson and Priscilla Tucker (University of Michigan Museum of Zoology). In addition, we would like to thank the Texas Tech HPCC (http://www.depts.ttu.edu/hpcc/) for providing the computational resources necessary to complete this project. Finally we would like to thank the reviewers. Their efforts greatly improved this manuscript.

References

Aberer A.J., Kobert K., Stamatakis A. 2014. ExaBayes: massively parallel Bayesian tree inference for the whole-genome era. Mol. Biol. Evol. 31:2553–2556.

Bayzid M.S., Mirarab S., Boussau B., Warnow T. 2015. Weighted statistical binning: enabling statistically consistent genome-scale phylogenetic analyses. PLoS One. 10:e0129183.

Bernt M., Donath A., Jühling F., Externbrink F., Florentz C., Fritzsch G., Pütz J., Middendorf M., Stadler P.F. 2013. MITOS: improved de novo metazoan mitochondrial genome annotation. Mol. Phylogenet. Evol. 69:313–319.

Bogdanowicz W., Piksa K., Tereba A. 2012. Hybridization hotspots at bat swarming sites. PLoS One 7:e53334.

Boyles J.G., Storm J.J. 2007. The perils of picky eating: dietary breadth is related to extinction risk in insectivorous bats. PLoS One 2:e672.

Caceres M.C., Barclay R.M.R. 2000. *Myotis septentrionalis*. Mamm. Species 634:1–4.
Carstens B.C., Dewey T.A. 2010. Species delimitation using a combined coalescent and information-theoretic approach: an example from North American *Myotis* bats. Syst Biol. 59:400–414.
Castresana J. 2000. Selection of conserved blocks from multiple alignments for their use in phylogenetic analysis. Mol. Biol. Evol. 17:540–552.
Chevreux B., Wetter T., Suhai S. 1999. Genome sequence assembly using trace signals and additional sequence information. Proceedings of the German Conference on Bioinformatics 99:45–56.
Chifman J., Kubatko L. 2014. Quartet inference from SNP data under the coalescent model. Bioinformatics 30:3317–3324.
Darriba D., Posada D. 2015. The impact of partitioning on phylogenomic accuracy. bioRxiv. Available from: URL https://doi.org/10.1101/023978.
DeGiorgio M., Degnan J.H. 2014. Robustness to divergence time underestimation when inferring species trees from estimated gene trees. Syst. Biol. 63:66–82.
Degnan J.H., Rosenberg N.A. 2009. Gene tree discordance, phylogenetic inference and the multispecies coalescent. Trends Ecol. Evol. 24:332–340.
Derti A., Roth F.P., Church G.M., Wu C.T. 2006. Mammalian ultraconserved elements are strongly depleted among segmental duplications and copy number variants. Nat. Genet. 38:1216–1220.
Douady C.J., Delsuc F., Boucher Y., Doolittle W.F., Douzery E.J.P. 2003. Comparison of Bayesian and maximum likelihood bootstrap measures of phylogenetic reliability. Mol. Biol. Evol. 20:248–254.
Dzeverin I. 2008. The stasis and possible patterns of selection in evolution of a group of related species from the bat genus *Myotis* (Chiroptera, Vespertilionidae). J. Mamm. Evol. 15:123–142.
Edwards S., Bensch S. 2009. Looking forwards or looking backwards in avian phylogeography? A comment on Zink and Carrowclough 2008. Mol. Ecol. 18:2930–2933.
Faircloth B.C. 2016. PHYLUCE is a software package for the analysis of conserved genomic loci. Bioinformatics 32:786–788.
Faircloth B.C., Branstetter M.G., White N.D., Brady S.G. 2015. Target enrichment of ultraconserved elements from arthropods provides a genomic perspective on relationships among Hymenoptera. Mol. Ecol. Resour. 15:489–501.
Faircloth B.C., McCormack J.E., Crawford N.G., Harvey M.G., Brumfield R.T., Glenn T.C. 2012. Ultraconserved elements anchor thousands of genetic markers spanning multiple evolutionary timescales. Syst. Biol. 61:717–726.
Findley J.S. 1972. Phenetic relationships among bats of the genus *Myotis*. Syst. Biol. 21:31–52.
Fitch J.H., Shump K.A. 1979. *Myotis keenii*. Mamm. Species Archive 121:1–3.
Glenn T.C., Nilsen R., Kieran T.J., Finger J.W., Pierson T.W., Bentley K.E., Hoffberg S., Louha S., Garcia-De-Leon F.J., Angel del Rio Portilla M., Reed K., Anderson J.L., Meece J.K., Aggery S., Rekaya R., Alabady M., Belanger M., Winker K., Faircloth B.C. 2016. Adapterama I: universal stubs and primers for thousands of dual-indexed Illumina libraries (iTru & iNext). bioRxiv. Available from: URL https://doi.org/10.1101/049114.
Good J.M., Vanderpool D., Keeble S., Bi K. 2015. Negligible nuclear introgression despite complete mitochondrial capture between two species of chipmunks. Evolution 69:1961–1972.
Gordon A., Hannon G. 2010. Fastx-toolkit. Available from: URL http://hannonlab.cshl.edu/fastx_toolkit.
Grabherr M.G., Haas B.J., Yassour M., Levin J.Z., Thompson D.A., Amit I., Adiconis X., Fan L., Raychowdhury R., Zeng Q., Chen Z., Mauceli E., Hacohen N., Gnirke A., Rhind N., di Palma F., Birren B.W., Nusbaum C., Lindblad-Toh K., Friedman N., Regev A. 2011. Full-length transcriptome assembly from RNA-Seq data without a reference genome. Nat. Biotech. 29:644–652.
Green R.E., Braun E.L., Armstrong J., Earl D., Nguyen N., Hickey G., Vandewege M.W., St. John J.A., Capella-Gutiérrez S., Castoe T.A., Kern C., Fujita M.K., Opazo J.C., Jurka J., Kojima K.K., Caballero J., Hubley R.M., Smit A.F., Platt R.N., Lavoie C.A., Ramakodi M.P., Finger J.W., Suh A., Isberg S.R., Miles L., Chong A.Y., Jaratlerdsiri W., Gongora J., Moran C., Iriarte A., McCormack J., Burgess S.C., Edwards S.V., Lyons E., Williams C., Breen M., Howard J.T., Gresham C.R., Peterson D.G., Schmitz J., Pollock D.D., Haussler D., Triplett E.W., Zhang G., Irie N., Jarvis E.D., Brochu C.A., Schmidt C.J., McCarthy F.M., Faircloth B.C., Hoffmann F.G., Glenn T.C., Gabaldón T., Paten B., Ray D.A. 2014. Three crocodilian genomes reveal ancestral patterns of evolution among archosaurs. Science 346:1254449.
Hahn C., Bachmann L., Chevreux B. 2013. Reconstructing mitochondrial genomes directly from genomic next-generation sequencing reads—a baiting and iterative mapping approach. Nucleic Acids Res. 41:e129.
Haynie M.L., Tsuchiya M.T.N., Ospina-Garcés S.M., Arroyo-Cabrales J., Medellín R.A., Polaco O.J., Maldonado J.E. 2016. Placement of the rediscovered *Myotis planiceps* (Chiroptera: Vespertilionidae) within the *Myotis* phylogeny. J. Mammal. 97:701–712.
Hedtke S.M., Townsend T.M., Hillis D.M. 2006. Resolution of phylogenetic conflict in large data sets by increased taxon sampling. Syst. Biol. 55:522–529.
Hollister N. 1909. Two new bats from the southwestern United States. Proc. Biol. Soc. Wash. 22:43–44.
Hosner P.A., Faircloth B.C., Glenn T.C., Braun E.L., Kimball R.T. 2016. Avoiding missing data biases in phylogenomic inference: An empirical study in the landfowl (Aves: Galliformes). Mol. Biol. Evol. 33:1110–1125.
Huang H., He Q., Kubatko L.S., Knowles L.L. 2010. Sources of error inherent in species-tree estimation: impact of mutational and coalescent effects on accuracy and implications for choosing among different methods. Syst. Biol. 59:573–583.
Huang W., Zhou G., Marchand M., Ash J.R., Morris D., Van Dooren P., Brown J.M., Gallivan K. A., Wilgenbusch J.C. 2016. TreeScaper: visualizing and extracting phylogenetic signal from sets of trees. Mol. Biol. Evol. 33:3314–3316.
Hudson R.R., Coyne J.A., Huelsenbeck J. 2002. Mathematical consequences of the genealogical species concept. Evolution 56:1557–1565.
Kapusta A., Suh A., Feschotte C. 2017. Dynamics of genome size evolution in birds and mammals. Proc. Natl. Acad. Sci. U. S. A. 114:E1460–E1469.
Katoh K., Misawa K., Kuma K.I., Miyata T. 2002. MAFFT: a novel method for rapid multiple sequence alignment based on fast Fourier transform. Nucleic Acids Res. 30:3059–3066.
Lack J.B., Roehrs Z.P., Stanley C.E., Ruedi M., Van Den Bussche R.A. 2010. Molecular phylogenetics of *Myotis* indicate familial-level divergence for the genus *Cistugo* (Chiroptera). J. Mammal. 91:976–992.
Lanfear R., Calcott B., Ho S.Y.W., Guindon S. 2012. PartitionFinder: combined selection of partitioning schemes and substitution models for phylogenetic analyses. Mol. Biol. Evol. 29: 1695–1701.
Larsen R.J., Knapp M.C., Genoways H.H., Khan F.A.A., Larsen P.A., Wilson D.E., Baker R.J. 2012. Genetic diversity of neotropical *Myotis* (Chiroptera: Vespertilionidae) with an emphasis on South American species. PLoS One 7:e46578.
LaVal R.K. 1973. A revision of the Neotropical bats of the genus *Myotis* Los Angeles County: Natural History Museum.
Leaché A.D., Rannala B. 2011. The accuracy of species tree estimation under simulation: a comparison of methods. Syst. Biol. 60: 126–137.
Leavitt D.H., Marion A.B., Hollingsworth B.D., Reeder T.W. 2017. Multilocus phylogeny of alligator lizards (Elgaria, Anguidae): testing mtDNA introgression as the source of discordant molecular phylogenetic hypotheses. Mol. Phylogenet. Evol. 110: 104–121.
Lewin-Koh N. 2011. Hexagon binning: an overview. Available from: URL ftp://ftp.naist.jp/pub/lang/R/CRAN/web/packages/hexbin/vignettes/hexagon_binning.pdf.
Li G., Davis B.W., Eizirik E., Murphy W.J. 2016. Phylogenomic evidence for ancient hybridization in the genomes of living cats (Felidae). Genome Res. 26:1–11.
Li H., Durbin R. 2009. Fast and accurate short read alignment with Burrows–Wheeler transform. Bioinformatics 25:1754–1760.
Liu L., Edwards S.V. 2015. Comment on "Statistical binning enables an accurate coalescent-based estimation of the avian tree". Science 350:171.

Liu L., Yu L., Kubatko L., Pearl D.K., Edwards S.V. 2009. Coalescent methods for estimating phylogenetic trees. Mol. Phylogenet. Evol. 53:320–328.

Manning R.W., Jones J.K. 1989. *Myotis evotis*. Mamm. Species Archive 329:1–5.

McCormack J.E., Harvey M.G., Faircloth B.C., Crawford N.G., Glenn T.C., Brumfield R.T. 2013. A Phylogeny of birds based on over 1,500 loci collected by target enrichment and high-throughput sequencing. PLoS One 8:e54848.

McGee M.D., Faircloth B.C., Borstein S.R., Zheng J., Darrin Hulsey C., Wainwright P.C., Alfaro M.E. 2016. Replicated divergence in cichlid radiations mirrors a major vertebrate innovation. Proc. R. Soc. Lond. B Biol. Sci. 283:20151413.

Meiklejohn K.A., Faircloth B.C., Glenn T.C., Kimball R.T., Braun E.L. 2016. Analysis of a rapid evolutionary radiation using Ultraconserved Elements: Evidence for a bias in some multispecies coalescent methods. Syst. Biol. 65:612–627.

Miller G.S. Jr., Allen G. 1928. The American bats of the genus *Myotis* and *Pixonyx*. Bull. US Nat. Mus. 144:1–218.

Mirarab S., Bayzid M.S., Boussau B., Warnow T. 2014. Statistical binning enables an accurate coalescent-based estimation of the avian tree. Science 346:1250463.

Mirarab S., Bayzid M.S., Warnow T. 2016. Evaluating summary methods for multilocus species tree estimation in the presence of incomplete lineage sorting. Syst. Biol. 65:366–380.

Mirarab S., Warnow T. 2015. ASTRAL-II: coalescent-based species tree estimation with many hundreds of taxa and thousands of genes. Bioinformatics 31:i44–i52.

Morales A.E., Jackson N.D., Dewey T.A., O'Meara B.C., Carstens B.C. 2016. Speciation with gene flow in North American *Myotis* bats. Syst. Biol. 66:440–452.

O'Farrell M.J., Studier E.H. 1980. *Myotis thysanodes*. Mamm. Species 137:1–5.

Pagan H.J.T., Smith J.D., Hubley R.M., Ray D.A. 2010. PiggyBac-ing on a Primate genome: novel elements, recent activity and horizontal transfer. Genome Biol. Evol. 2:293–303.

Pattengale N.D., Alipour M., Bininda-Emonds O.R.P., Moret B.M.E., Stamatakis A. 2009. How many bootstrap replicates are necessary? In: Batzoglou S, editor. Research in Computational Molecular Biology: 13th Annual International Conference, RECOMB 2009, Tucson, AZ, USA, May 18-21, 2009. Proceedings. Berlin, Heidelberg: Springer Berlin Heidelberg, p. 184–200.

Piaggio A.J., Valdez E.W., Bogan M.A., Spicer G.S. 2002. Systematics of *Myotis occultus* (Chiroptera: Vespertilionidae) inferred from sequences of two mitochondrial genes. J. Mammal. 83:386–395.

Platt R.N., Mangum S.F., Ray D.A. 2016. Pinpointing the vesper bat transposon revolution using the Miniopterus natalensis genome. Mob. DNA 7:12.

Platt R.N., Vandewege M.W., Kern C., Schmidt C.J., Hoffmann F.G., Ray D.A. 2014. Large numbers of novel miRNAs originate from DNA transposons and are coincident with a large species radiation in bats. Mol. Biol. Evol. 31:1536–1545.

Platt R.N., Zhang Y., Witherspoon D.J., Xing J., Suh A., Keith M.S., Jorde L.B., Stevens R.D., Ray D.A. 2015. Targeted capture of phylogenetically informative ves SINE insertions in genus myotis. Genome Biol. Evol. 7:1664–1675.

Pritham E.J., Feschotte C. 2007. Massive amplification of rolling-circle transposons in the lineage of the bat *Myotis* lucifugus. Proc. Natl. Acad. Sci. U. S. A. 104:1895–1900.

Puechmaille S.J., Allegrini B., Boston E.S.M., Dubourg-Savage M.-J., Evin A., Knochel A., Le Bris Y., Lecoq V., Lemaire M., Rist D., Teeling E.C. 2012. Genetic analyses reveal further cryptic lineages within the *Myotis nattereri* species complex. Mammal. Biol. 77:224–228.

Rambaut A., Drummond A. 2013. TreeAnnotator v1. 7.0. Available from: URL http://beast.bio.ed.ac.uk.

Rambaut A., Suchard M., Xie D., Drummond A. 2014. Tracer v1.6. Available from: URL http://beast.bio.ed.ac.uk.

Ray D.A., Feschotte C., Pagan H.J.T., Smith J.D., Pritham E.J., Arensburger P., Atkinson P.W., Craig N.L. 2008. Multiple waves of recent DNA transposon activity in the bat, *Myotis lucifugus*. Genome Res. 18:717–728.

Ray D.A., Pagan H.J.T., Thompson M.L., Stevens R.D. 2007. Bats with hATs: evidence for recent DNA transposon activity in genus *Myotis*. Mol. Biol. Evol. 24:632–639.

Rice P., Longden I., Bleasby A. 2000. EMBOSS: the European molecular biology open software suite. Curr. Trends 16:276–277.

Rodríguez-Ezpeleta N., Brinkmann H., Roure B., Lartillot N., Lang B.F., Philippe H. 2007. Detecting and overcoming systematic errors in genome-scale phylogenies. Syst. Biol. 56:389–399.

Roehrs Z.P., Lack J.B., Van Den Bussche R.A. 2010. Tribal phylogenetic relationships within Vespertilioninae (Chiroptera: Vespertilionidae) based on mitochondrial and nuclear sequence data. J. Mammal. 91:1073–1092.

Ruedi M., Mayer F. 2001. Molecular systematics of bats of the genus *Myotis* (Vespertilionidae) suggests deterministic ecomorphological convergences. Mol. Phylogenet. Evol. 21:436–448.

Ruedi M., Stadelmann B., Gager Y., Douzery E.J.P., Francis C.M., Lin L.-K., Guillén-Servent A., Cibois A. 2013. Molecular phylogenetic reconstructions identify East Asia as the cradle for the evolution of the cosmopolitan genus *Myotis* (Mammalia, Chiroptera). Mol. Phylogenet. Evol. 69:437–449.

Seo T.-K. 2008. Calculating bootstrap probabilities of phylogeny using multilocus sequence data. Mol. Biol. Evol. 25:960–971.

Simões B.F., Rebelo H., Lopes R.J., Alves P.C., Harris D.J. 2007. Patterns of genetic diversity within and between *Myotis d. daubentonii* and *M. d. nathalinae* derived from cytochrome *b* mtDNA sequence data. Acta Chiropt. 9:379–389.

Sota T. 2002. Radiation and reticulation: extensive introgressive hybridization in the carabid beetles *Ohomopterus* inferred from mitochondrial gene genealogy. Population Ecol. 44: 0145–0156.

Stadelmann B., Lin L.K., Kunz T.H., Ruedi M. 2007. Molecular phylogeny of New World *Myotis* (Chiroptera, Vespertilionidae) inferred from mitochondrial and nuclear DNA genes. Mol. Phylogenet. Evol. 43:32–48.

Stamatakis A. 2006. RAxML-VI-HPC: maximum likelihood-based phylogenetic analyses with thousands of taxa and mixed models. Bioinformatics 22:2688–2690.

Swofford D.L. 2003. PAUP*. Phylogenetic analysis using parsimony (* and other methods). Version 4. http://paup.sc.fsu.edu/

Thomas J., Sorourian M., Ray D., Baker R.J., Pritham E.J. 2011. The limited distribution of Helitrons to vesper bats supports horizontal transfer. Gene 474:52–58.

Vachaspati P., Warnow T. 2015. ASTRID: Accurate Species TRees from Internode Distances. BMC Genomics 16:S3.

Valdez E.W., Choate J.R., Bogan M.A., Yates T.L. 1999. Taxonomic status of *Myotis occultus*. J. Mammal. 80:545–552.

Warner R.M. 1982. *Myotis auriculus*. Mamm. Species 191:1–3.

Wiens J.J., Kuczynski C.A., Smith S.A., Mulcahy D.G., Sites J.J.W., Townsend T.M., Reeder T.W. 2008. Branch lengths, support, and congruence: testing the phylogenomic approach with 20 nuclear loci in snakes. Syst. Biol. 57:420–431.

Willis S.C., Farias I.P., Ortí G. 2014. Testing mitochondrial capture and deep coalescence in Amazonian cichlid fishes (Cichlidae: *Cichla*). Evolution 68:256–268.